coatings

MDPI

Article

The Microstructures and Wear Resistance of CoCrFeNi_2Mo_x High-Entropy Alloy Coatings

Hui Liang [1], Jinxin Hou [2,*], Jianhong Liu [1], Hongtai Xu [1], Yaning Li [3], Li Jiang [3] and Zhiqiang Cao [3,*]

[1] School of Physics and Electronic Technology, Liaoning Normal University, Dalian 116029, China
[2] Editorial Department of Journal of Liaoning Normal University, Liaoning Normal University, Dalian 116029, China
[3] Key Laboratory of Solidification Control and Digital Preparation Technology (Liaoning Province), School of Materials Science and Engineering, Dalian University of Technology, Dalian 116024, China
* Correspondence: jxhou@lnnu.edu.cn (J.H.); caozq@dlut.edu.cn (Z.C.)

Abstract: The CoCrFeNi_2Mo_x ($x = 0$, 0.4, 0.5, 1.0, x values in atomic ratio) high-entropy alloy coatings were designed and prepared on the Ti-6Al-4V substrate by laser cladding technology, their microstructures, and dry sliding wear resistance were studied in detail. When $x < 0.4$, the coatings were mainly composed of BCC solid solution phase, (Ni, Co)Ti_2 phase, and α-Ti phase. When $x \geq 0.4$, the new σ phase appeared in the coatings. As the Mo content increases from 0 to 1.0, the hardness showed a trend of first increasing and then decreasing, especially when $x = 0.5$, the coating hardness reached its maximum (882 HV), which was 2.65 times the hardness of the Ti-6Al-4V substrate. The CoCrFeNi_2Mo_x high-entropy alloy coatings significantly improved the wear resistance of Ti-6Al-4V substrate, and with the increase in Mo content, the friction coefficient, widths/depths of worn tracks and wear rates of the coatings showed a trend of first decreasing and then increasing. In particular, when $x = 0.5$, the CoCrFe$Ni_2Mo_{0.5}$ high-entropy alloy coating has the lowest friction coefficient (0.63), widths/depths of worn tracks (width: 803.690 μm; depth: 20.630 μm) and wear rate (5.136×10^{-5} mm^3/(N·m)), which is one order of magnitude smaller than that of the substrate (3.694×10^{-4} mm^3/(N·m)), demonstrating the best wear resistance. This is mainly because the appropriate proportion of hard α-Ti and σ phases effectively played a supporting role in resisting wear, while the relatively soft and dispersed BCC and (Ni, Co)Ti_2 phases could effectively prevent the occurrence of brittle fracture during wear test process.

Keywords: high-entropy alloy; micro-structures; dry-sliding; wear

check for updates

Citation: Liang, H.; Hou, J.; Liu, J.; Xu, H.; Li, Y.; Jiang, L.; Cao, Z. The Microstructures and Wear Resistance of CoCrFeNi_2Mo_x High-Entropy Alloy Coatings. *Coatings* **2024**, *14*, 760. https://doi.org/10.3390/coatings14060760

Academic Editor: Cecilia Bartuli

Received: 1 May 2024
Revised: 8 June 2024
Accepted: 14 June 2024
Published: 15 June 2024

1. Introduction

Wear is one of the main causes of material failure, and approximately 80% of mechanical equipment parts in the world are damaged due to various forms of wear [1]. This not only causes a significant loss of resources but also poses a huge threat to life and safety. Therefore, the preparation of wear-resistant coating materials on the surface of mechanical equipment parts is one of the key methods to effectively solve the above problems. Compared to other coating preparation methods, such as thermal or cold spraying, plasma spraying, magnetron sputtering, and spark plasma sintering, laser cladding technology can adjust the coating thickness in a large range of micrometers to millimeters, obtain dense cladding structure, and achieve good metallurgical bonding between the coating and the substrate [2]. Due to its versatility and the high heating (cooling) rate (approximately 106 K/s), laser cladding technology can accurately adjust surface properties according to service requirements while retaining the overall mechanical properties of the material, thus obtaining coatings with excellent performances, which has attracted increasing attention [3], indicating that laser cladding technology is a superior method for preparing wear-resistant coatings.

In addition, the selection of appropriate wear-resistant materials in equipment processing, manufacturing, and production processes is of great significance for reducing production costs, improving work efficiency, and promoting the development of the national economy. So far, more than 30 alloy systems such as Ni-based alloys and Al alloys have been widely used in industrial production. As traditional alloy materials, they are based on a certain metal element, and different alloy elements are added according to the performance requirements. However, with the development of modern industry, traditional alloys can no longer fully meet practical needs [4,5]. Therefore, in the 1990s, researchers proposed the concept of a new type of high-entropy alloy, which is an alloy material system composed of 5~13 elements in equal or nearly equal atomic ratios [6–8]. Due to the close molar fractions of each component in high-entropy alloys, the resulting alloy system has a high mixing entropy value. According to the Gibbs free energy formula $\Delta G = \Delta H - T\Delta S$, a higher mixing entropy is beneficial for maintaining the Gibbs free energy of the system at a lower level, making it easier to form relatively simple phase compositions [9,10]. Meanwhile, the high entropy effect generated by multi-principal component mixing can improve the compatibility of elements [11,12]. In addition, the hysteresis diffusion effect, lattice distortion effect, and "cocktail" effect caused by the different atomic lattice sizes and combinations of different elements ensure that high-entropy alloys have excellent properties such as high hardness and wear resistance and have enormous industrial application potential and academic research value [13–15]. Wang et al. [16] used laser cladding technology to prepare $Al_{0.4}CoCuNiSi_{0.2}Ti_{0.25}$ high-entropy alloy coating on the surface of 45 steel. The coating is mainly composed of BCC and FCC phases, with a small amount of Ni-Ti-Si intermetallic compound generated. Due to the effects of solid solution strengthening and fine-grained strengthening, the cladding layer has a higher hardness and exhibits good wear resistance. Qi et al. [17] used mechanical alloying technology combined with laser cladding technology to prepare ultrafine-grained NbMoTaW high-entropy alloy powder and its coating with a simple BCC solid solution structure. The thickness of the laser cladding coating reached 0.8 mm. After laser cladding, the alloy elements underwent slight segregation, mainly composed of the BCC1 phase (rich in Mo and W elements) and BCC2 phase (rich in Nb and Ta elements). Due to the effects of solid solution strengthening and fine-grained strengthening, the surface hardness of the coating has been greatly improved. Zheng et al. [18] prepared NiCoFeCrTi high-entropy alloy using laser cladding technology and analyzed its microstructure and properties. The results indicated that the coating was metallurgical bonded to the substrate, with no pores or cracks, and the microstructure was composed of FCC phase, exhibiting excellent wear resistance. Huang et al. [19] successfully prepared the $CoCrCuFeNiTi_x$ high-entropy alloy coatings on the surface of #45 steel substrate using laser cladding technology. The microstructure and tribological properties at 600 °C were studied. As a result, when x = 1.5, a TiO_2 protective layer was formed on the worn surface of the coating, which effectively suppressed wear damage and exhibited optimal wear resistance. Wu et al. [20] prepared $Al_2CrFeNiMo_x$ high-entropy alloy coatings on a stainless steel substrate and found that the coatings were composed of two BCC solid solution phases. With the increase in Mo content, the hardness of the coatings gradually increased. The hardness of $Al_2CrFeNiMo_2$ coating reached 687 HV, which was three times the hardness of the substrate (243 HV). However, the wear resistance of the coating did not increase with the increase in Mo content. $Al_2CrFeNiMo$ coating had the best wear resistance because the wear resistance of the coatings was not only related to hardness but also to the plasticity and toughness of the coatings. Coatings with high hardness but high brittleness would have poorer wear resistance.

Based on this, in this article, $CoCrFeNi_2Mo_x$ (x = 0, 0.4, 0.5, 1.0, x values in atomic ratio) high-entropy alloy coatings are designed and prepared using laser cladding technology on Ti-6Al-4V substrate, the microstructures and dry sliding wear resistance of coatings are studied in detail, which not only has important theoretical value for the development of new type wear-resistant high-entropy alloy coatings but also plays a powerful role in promoting the application of high-entropy alloy materials in the field of mechanical engineering.

2. Materials and Methods

2.1. Experiment Materials and Preparation

Although Ti-6Al-4V titanium alloy has a significant position in aerospace, biomedical, and other fields, its poor wear resistance, to some extent, limits development. Therefore, in order to expand the application range of this titanium alloy and promote its development, surface modification has become a top priority. So, in this article, the Ti-6Al-4V (TC4) titanium alloy was selected as the substrate material; its composition is Al 5.5~6.8 wt.%, Si 0.15 wt.%, V 3.4~4.5 wt.%, O 0.2 wt.%, N 0.05 wt.%, C 0.1 wt.%, Fe 0.3 wt.%, H 0.01 wt.%, Ti balance. Before the experiment, the substrate was first cut into a rectangular prism with a size of 90 mm × 12 mm × 9 mm. Then, the surface of TC4 substrate was treated with sandpapers from 80 # to 600 # to remove surface oil stains and oxide layers. It was subsequently cleaned by ultrasound and dried with a hair dryer. According to the composition of the designed $CoCrFeNi_2Mo_x$ (x = 0, 0.4, 0.5, 1.0, x values in atomic ratio, recorded as Mo0, Mo0.4, Mo0.5, Mo1.0) high-entropy alloy coatings, the specific composition of each element is shown in Table 1, Co, Cr, Fe, Ni, and Mo raw material powders were weighed using an electronic balance with a sensitivity of 0.0001 g. The particle sizes of the raw material powders were approximately 75 μm, the purity was greater than 99.97%. The planetary ball mill was used to uniformly mix the above-mentioned raw material powders, the rotational speed was 175 rpm, and the time was 1 h. Uniformly mixed high-entropy alloy powders were placed on the TC4 substrate to form the powder bed with thick of 1.2 mm for subsequent laser cladding experiments. The laser cladding process was carried out using the preset powder method, and the equipment used was an LDF-4000-100 semiconductor laser (Laserline, Mülheim-Kärlich, Germany). The experimental parameters were spot diameter of 3 mm, laser power of 1000 W, scanning speed of 5 mm/s, and argon gas flow rate of 5 L/min.

Table 1. The specific composition of each element in $CoCrFeNi_2Mo_x$ coatings.

Samples	Samples	Atomic Percent/at.%	Mass Percent/wt.%	Mass/g (Total Mass = 20 g)
Mo0	Co	1.0	20.7397	4.1479
	Cr	1.0	18.2984	3.6597
	Fe	1.0	19.6536	3.9307
	Ni	2.0	41.3083	8.2617
Mo0.4	Co	1.0	18.2720	3.6544
	Cr	1.0	16.1212	3.2242
	Fe	1.0	17.3152	3.4630
	Ni	2.0	36.3933	7.2787
	Mo	0.4	11.8983	2.3797
Mo0.5	Co	1.0	17.7442	3.5488
	Cr	1.0	15.6555	3.1311
	Fe	1.0	16.8150	3.3630
	Ni	2.0	35.3420	7.0684
	Mo	0.5	14.4433	2.8887
Mo1.0	Co	1.0	15.5048	3.1010
	Cr	1.0	13.6797	2.7359
	Fe	1.0	14.6929	2.9386
	Ni	2.0	30.8817	6.1763
	Mo	1.0	25.2410	5.0482

2.2. Materials Characterization

The phase compositions of $CoCrFeNi_2Mo_x$ high-entropy alloy coatings were analyzed using X-ray diffraction technology (XRD). The X-ray diffractometer used in the experiment is the EMPYREAN diffractometer produced in Almelo, The Netherlands. The parameters set for this detection were Cu-Kα Radiation (wavelength $\lambda = 1.5406$ μm), scanning angle of

20°~100°, working current of 40 mA, working voltage of 40 KV, and a scanning speed of 0.33°/s. The microstructures of $\mathrm{CoCrFeNi_2Mo_x}$ high-entropy alloy coatings were analyzed using scanning electron microscopy (SEM, a ZEISS Supra 55 field emission scanning electron microscope produced by Zeiss in Jena, Germany). In addition, the built-in energy spectrum analyzer (EDS) of this device was used for detecting and analyzing the micro-components of the samples. Before testing, the $\mathrm{CoCrFeNi_2Mo_x}$ high-entropy alloy coatings were cut into rectangular shapes of 6 mm × 12 mm × 9 mm by wire cutting, and their cross-sections were sequentially sanded and polished with sandpaper and diamond grinding paste. Subsequently, the tested surfaces of the coatings were corroded with a self-prepared corrosion solution ($\mathrm{HF:HNO_3}$ = 3:1). In addition, electron probe microscopy (EPMA) technology was used to analyze the microstructures and distribution of various elements in different phases of coatings. The equipment used in this experiment was the JXA-8530F field emission electron probe produced by JOEL in Tokyo, Japan.

2.3. Materials Testing

The MH-50 Vickers hardness tester produced by Shanghai Hengyi Precision Instrument Co., Ltd. in Shanghai, China was used to measure the hardness of $\mathrm{CoCrFeNi_2Mo_x}$ high-entropy alloy coatings. The test parameters were set to a loading load of 1000 g and a holding time of 15 s. The sliding friction and wear tests were conducted using the CFT-I material surface performance comprehensive tester produced by Zhongke Kaihua Company in Lanzhou, China. The process was carried out at room temperature and dry conditions, using $\mathrm{Si_3N_4}$ balls (with a diameter of 4 mm and a Vickers hardness of about 1500 HV) as the coupled balls. The friction and wear test parameters were set as follows: rotational speed of 400 r/min, loading time of 900 s, reciprocating sliding distance of 5 mm, and loading load of 13 N. Each sample should undergo at least three repeated tests to ensure the accuracy of the data. The LEXT OLS4000 laser confocal microscope produced by Japan's Olympus company (Tokyo, Japan) was used to measure the widths and depths of the samples' worn tracks after wear tests, and then the wear rates were calculated according to the formula $\delta = \frac{S \times L}{FL'}$ (the δ represents wear rate, S represents the cross-sectional area of the worn track, L represents the reciprocating distance, F represents the load, and L′ represents the total reciprocating distance of sliding) [21].

3. Results and Discussion

3.1. Phase Constitution

Figure 1a shows the XRD results of $\mathrm{CoCrFeNi_2Mo_x}$ high-entropy alloys. It can be seen that when $x < 0.4$, the coatings are mainly composed of BCC solid solution phase, $\mathrm{(Ni, Co)Ti_2}$ phase, and α-Ti phase. When $x > 0.4$, the new diffraction peak appeared in the coatings, which is found to be the σ phase. Based on the Gibbs phase ratio $F = C - P + 1$ (F is the degree of freedom, C is the number of main elements, and P is the number of phases) [22], it can be inferred that the $\mathrm{CoCrFeNi_2Mo_x}$ high-entropy alloy coating system with five elements should contain seven phases [23]. Obviously, this is inconsistent with the above results. The reason is that the $\mathrm{CoCrFeNi_2Mo_x}$ high-entropy alloy coatings have a unique high-entropy effect [24]. According to the formula $\Delta G_{mix} = \Delta H_{mix} - T\Delta S_{mix}$ (ΔG_{mix} is Gibbs free energy, ΔH_{mix} is the mixing enthalpy of the system, ΔS_{mix} is the mixing entropy of the system, and T is the temperature) [25], when ΔH_{mix} remains constant, the high ΔS_{mix} of the $\mathrm{CoCrFeNi_2Mo_x}$ high-entropy alloy coatings would promote a decrease in the ΔG_{mix} of the system, and the lower ΔG_{mix} value would promote the formation of simple solid solution phases in the high-entropy alloy coatings, thus leading to a decrease in the number of phases of $\mathrm{CoCrFeNi_2Mo_x}$ high-entropy alloy coatings. In addition, as shown in Figure 1b, after amplifying the $(110)_{\mathrm{BCC}}$ peak, it can be found that as the Mo content increases, the diffraction peak of the BCC phase is shifted. When x increases from 0 to 0.4, this diffraction peak first shifts to the right and then shifts to the left again as x continues to increase. According to the Bragg equation $2d\sin\theta = n\lambda$ and lattice constant calculation formula $a = d\sqrt{h^2+k^2+l^2}$, when the $(110)_{\mathrm{BCC}}$ diffraction peak shifts to the right, that is, as the θ increases, the interplanar spacing d would decrease, and its lattice constant would also decrease. Subsequently, when the diffraction peak of $(110)_{BCC}$ shifts to the left, its lattice constant correspondingly increases. The specific values of the lattice constant of the BCC phase were further calculated using Jade 6.5 software, as shown in Table 2. This further confirms the trend of lattice constant variation; that is, with the increase in Mo content, the lattice constant of the BCC phase first decreases and then increases. The reason for this phenomenon is that when a small amount of Mo atoms are added, they first replace the Ti atoms with radii larger than Mo, promoting a decrease in lattice constant. Subsequently, with the addition of a large number of Mo atoms, the excess Mo atoms gradually begin to replace the atoms with radii smaller than Mo itself, then leading to an increase in lattice constant. On the other hand, this may also be due to the presence of residual stress within the coatings, causing lattice distortion, ultimately leading to these shifts in the diffraction peak position.

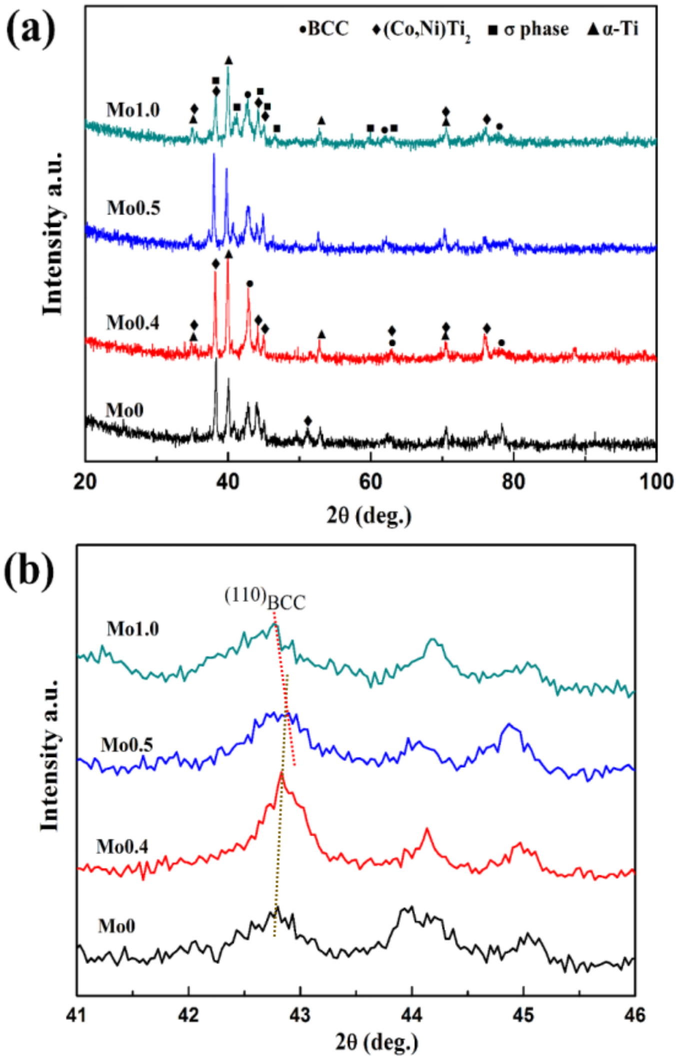

Figure 1. XRD patterns of the $CoCrFeNi_2Mo_x$ coatings: (**a**) XRD patterns, (**b**) magnification of (110) BCC peaks.

Table 2. The lattice parameters of BCC phase of CoCrFeNi$_2$Mo$_x$ coatings (a/Å).

Samples	Phase	Lattice Constant a/Å			
		(110)	(200)	(211)	Average Value
Mo0	BCC	2.1134	1.4923	1.2198	1.6085
Mo0.4	BCC	2.1088	1.4800	1.2299	1.6062
Mo0.5	BCC	2.1112	1.4944	1.2241	1.6099
Mo1.0	BCC	2.1144	1.4969	1.2207	1.6106

3.2. Microstructures

Figure 2 is the SEM images of the typical cross-section of CoCrFeNi$_2$Mo$_x$ high-entropy alloy coatings. Figure 2a shows that the coating is divided vertically from top to bottom into a cladding zone (abbreviated "CZ"), bonding zone (abbreviated "BZ"), heat affected zone (abbreviated "HAZ"), and TC4 substrate material (abbreviated "substrate") [26]. Figure 2b is an enlarged view of the bonding zone. It is evident that the coating undergoes a longitudinal transition from planar crystals to columnar crystals from bottom to top in the crystal growth mode of the bonding zone. According to the solidification theory [27], the ratio of temperature gradient G and solidification rate R is an important factor that directly determines the growth mode of crystals. More specifically, at the bottom of the melt pool (i.e., at the solid–liquid interface), the former (temperature gradient G) has a large value, while the value of the latter (solidification rate R) is very small, resulting in a large ratio of (i.e., G/R). As a result, the phenomenon of component undercooling would be difficult to occur. In addition, the surface of the TC4 substrate material is in a semi-molten state near this region, which is prone to nucleation, and the nucleation rate would be greater than the growth rate, ultimately exhibiting a planar growth state. During the continuous advancement of the solid–liquid interface, the values of G and R show a decreasing and increasing trend, respectively; that is, the value of G/R shows a gradually decreasing trend. At the same time, the solute concentration C_0 gradually increases, making it easy for component undercooling to occur, leading to the transformation of crystal growth in this area from planar to columnar [28].

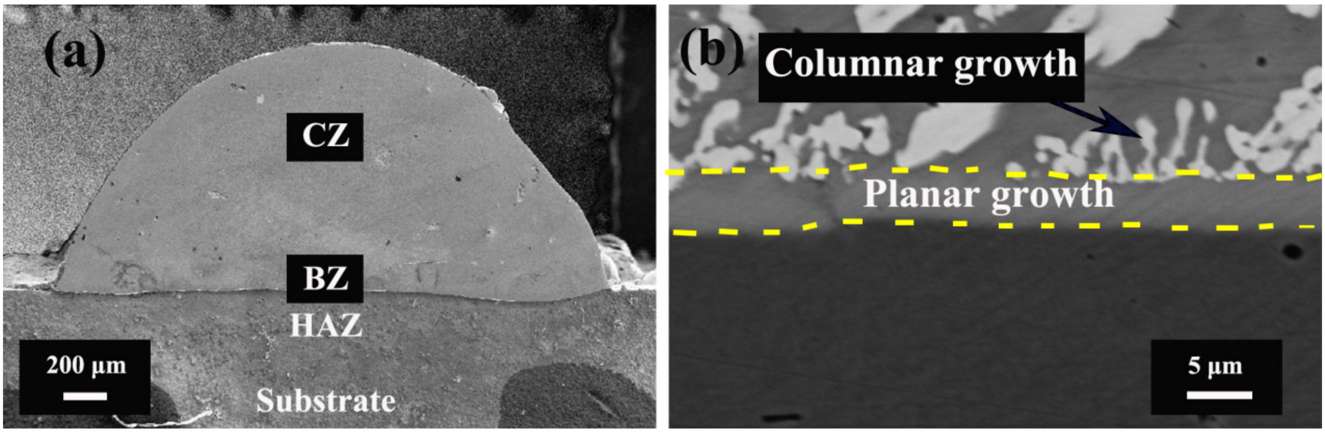

Figure 2. Typical cross-section views of CoCrFeNi$_2$Mo$_x$ coatings: (**a**) macro cross-sectional view; (**b**) the view near fusion line.

As shown in Figure 3, the EPMA images of the cladding zone of CoCrFeNi$_2$Mo$_x$ high-entropy alloy coatings all show the typical dendritic morphology. When $x \leq 0.4$, the coatings are mainly composed of three phases: dendritic DR (denoted as A), interdendritic ID (denoted as B), and black phase (denoted as C). And with the increase in Mo content, the content of the dendritic phase (A) shows an increasing trend. When the Mo content increases to 0.5, the microstructure of the coating undergoes significant changes; that is, the white phase (D) precipitates in the interdendritic region (B), which means that an increase in Mo content will promote the formation of a new phase. And as the Mo content continues to increase to 1.0, the white phase (D) significantly increases and coarsens, becoming a block-like structure. The EDS results (Table 3) and Figure 4 show that the dendritic region (A) is mainly enriched with Fe and Cr elements, and the interdendritic region (B) is enriched with Co, Ni, and Ti phases. Based on XRD results and previous reports [29,30], it can be preliminarily inferred that the dendritic region (A) is the BCC solid solution phase, and the interdendritic region (B) is the (Co, Ni)Ti_2 phase. Region C is enriched with a large amount of Ti element, and it can be inferred from XRD results that this phase is a type of α-Ti phase. At the same time, it is worth noting that the $CoCrFeNi_2Mo_x$ high-entropy alloy coatings do not contain Ti elements. The main reason for this phenomenon of the appearance of a large number of Ti elements is that a large amount of thermal energy is input during the laser cladding process, and the TC4 substrate near the bonding zone is rapidly melted, forming a common melt pool with the melted $CoCrFeNi_2Mo_x$ powders. They rapidly form convection in the molten pool; moreover, along with their rapid cooling to form coatings, there is also the mutual diffusion of elements between the coatings and the TC4 substrate, resulting in the appearance of a large amount of Ti element inside the coatings, which further proves the formation of good metallurgical bonding between the coatings and the TC4 substrate. In addition, Table 3 shows that the white phase (D) is enriched with Fe, Cr, and Mo elements. Much of the previous literature reports that high-entropy alloy systems containing Mo elements are prone to the formation of the σ phase [31–34]. Further combined with XRD results, it can be determined that the white phase (region D) is the FeCrMo-type σ phase. It is worth mentioning that with the increase in Mo content, the dendritic phase (A) shows an increasing trend, while the white phase (D) not only increases in content but also becomes a coarse block-like structure. This further proves that the addition of Mo element can easily promote the formation of the BCC phase and σ phase, and in this alloy system, the maximum solid solubility of Mo element in the BCC phase is between x = 0.4 and x = 0.5.

Table 3. The chemical compositions of $CoCrFeNi_2Mo_x$ coatings (at.%).

Sample	Region	Co	Cr	Fe	Ni	Mo	Ti
Mo0	A	15.91	23.79	19.98	19.66	...	20.66
	B	19.76	7.33	11.01	36.34	...	25.56
	C	6.33	6.21	6.50	12.64	...	68.32
Mo0.4	A	11.77	21.45	21.08	15.73	8.34	21.63
	B	16.95	6.38	9.96	38.35	4.16	24.20
	C	6.18	6.29	5.15	9.54	2.63	70.21
Mo0.5	A	8.56	22.21	17.25	16.09	7.06	28.83
	B	13.83	5.57	9.86	22.32	4.79	43.63
	C	5.93	6.98	6.31	10.13	3.29	67.36
	D	2.71	19.54	25.51	3.31	23.62	25.31
Mo1.0	A	14.06	18.92	15.21	16.17	8.05	27.59
	B	18.72	5.52	8.21	21.74	4.40	41.41
	C	6.01	6.05	6.27	11.11	6.20	64.36
	D	2.11	16.98	23.14	1.92	38.23	17.62

3.3. Microhardness

Figure 5 shows the hardness distribution of $CoCrFeNi_2Mo_x$ high-entropy alloy coatings. Obviously, the average hardness values of Mo0, Mo0.4, Mo0.5, and Mo1.0 coatings are 785 HV, 850 HV, 882 HV, and 813 HV, respectively, which is much higher than the hardness of TC4 substrate (about 320 HV), almost 2.45–2.65 times that of the substrate. This is mainly attributed to the following points. Firstly, the laser cladding process with rapid heating and solidification characteristics can easily induce $CoCrFeNi_2Mo_x$ high-entropy alloy coatings to exhibit finer microstructures, playing a role in fine-grain strengthening. Secondly, the $CoCrFeNi_2Mo_x$ high-entropy alloy coatings themselves contain a large number of principal elements, and there is a large atomic radius difference between the atoms, which promotes the occurrence of severe lattice distortion and effectively plays a role in solid solution strengthening [35]. Furthermore, the precipitation of a Ti-rich phase in $CoCrFeNi_2Mo_x$ high-entropy alloy coatings plays a role in second-phase strengthening. It can be seen that under the combined effect of the above three factors, the $CoCrFeNi_2Mo_x$ high-entropy alloy coatings exhibit high hardness. In addition, as the Mo content increases from 0 to 1.0, the hardness shows a trend of first increasing and then decreasing. Especially when x = 0.5, the coating hardness reaches a maximum (882 HV), which is 2.65 times the hardness of the TC4 substrate. Specifically, as the Mo content increases from 0 to 0.4, more Mo atoms with larger atomic radii gradually dissolve into BCC, causing severe lattice distortion and enhancing the solid solution strengthening effect, resulting in a significant increase in Mo0.4 hardness compared to Mo0. Then, as the Mo content continues to increase to 0.5, the hard FeCrMo-type σ phase (TCP structure) begins to appear in the coating, which also causes the second phase strengthening, directly leading to a further increase in the hardness of the coating. When Mo content was further added to 1.0, the hardness of the coating showed a decreasing trend. This is because the σ phase in Mo1.0 coating becomes too coarse and blocky, which actually weakens the effect of fine-grained strengthening. At this time, the effect of second phase strengthening is insufficient to compensate for the above point, resulting in a decreasing trend in the hardness of the Mo1.0 coating.

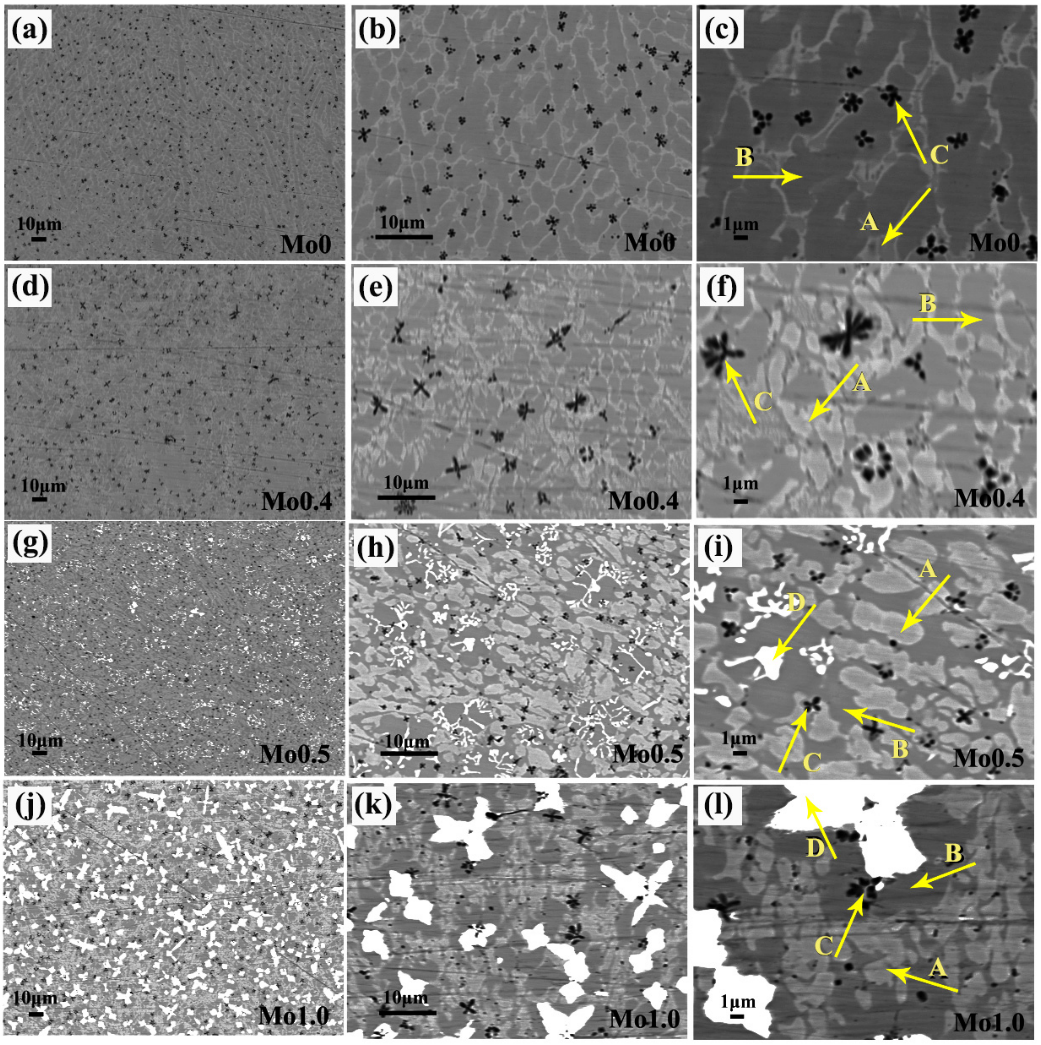

Figure 3. Electron probe backscatter images of $CoCrFeNi_2Mo_x$ coatings: (**a**–**c**) Mo0, (**d**–**f**) Mo0.4, (**g**–**i**) Mo0.5, (**j**–**l**) Mo1.0.

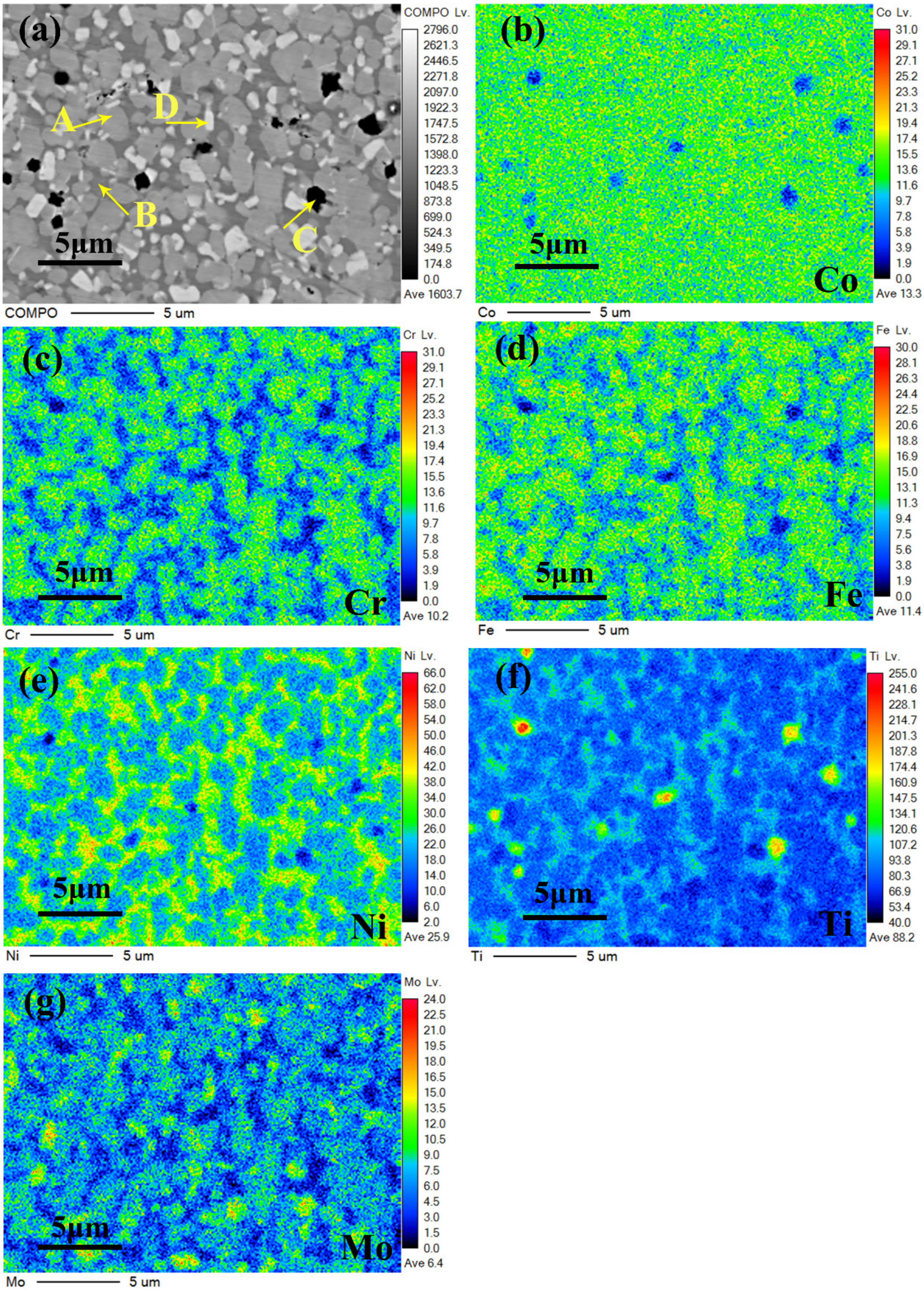

Figure 4. EPMA mapping results of $CoCrFeNi_2Mo_{0.5}$ coating: (**a**) backscattered electron image, (**b**) Co, (**c**) Cr, (**d**) Fe, (**e**) Ni, (**f**) Ti, (**g**) Mo.

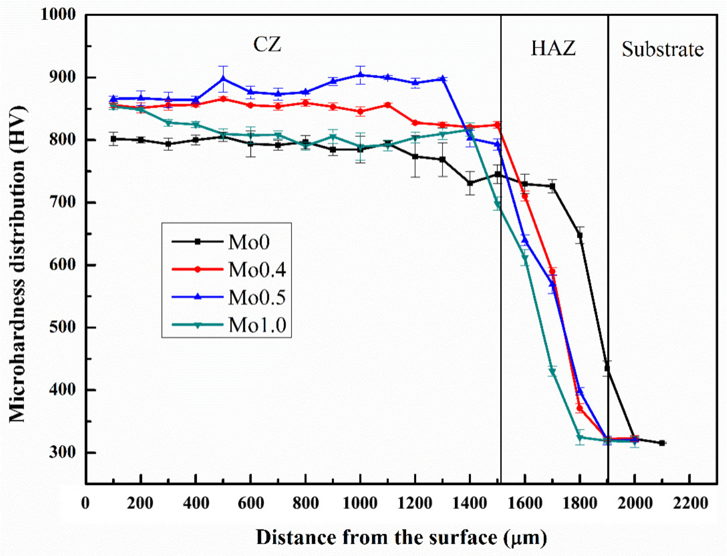

Figure 5. The microhardness of $CoCrFeNi_2Mo_x$ coatings.

3.4. Wear Resistance

Figures 6 and 7 show the results of the friction and wear behaviors of samples, respectively. And Figure 8 is the 3D worn morphologies of samples. In Figure 6, the fluctuation and average values of the friction coefficients of all coatings are smaller compared to the TC4 substrate material, indicating the better friction behaviors of coatings. Additionally, as for the coatings, the friction coefficient values show a trend of first decreasing ($x \leq 0.5$) and then increasing ($x > 0.5$); especially when $x = 0.5$, the friction coefficient fluctuation of the $CoCrFeNi_2Mo_{0.5}$ coating is the smallest, and its average value is the lowest (0.63), showing the optimal friction behavior. In addition, from Figures 7 and 8, it can be intuitively seen that the widths/depths of worn tracks and wear rates of all $CoCrFeNi_2Mo_x$ high-entropy alloy coatings are much lower than those of the substrate material, indicating that the coatings have a significant effect on improving the wear resistance of TC4 substrate. As for the $CoCrFeNi_2Mo_x$ high-entropy alloy coatings, with the increase in Mo content, the widths/depths of worn tracks and wear rates of the $CoCrFeNi_2Mo_x$ high-entropy alloy coatings show a trend of first decreasing and then increasing. That is, when $x \leq 0.5$, the widths/depths of worn tracks and wear rates of the coatings show a gradually decreasing trend, which means that their wear resistance gradually increases. As x continues to increase to 1.0, the widths/depths of worn tracks and wear rates of the coatings show a decreasing trend, and the wear resistance gradually weakens. Based on the classic Archard's law in the field of tribology, the wear resistance of metal materials is positively correlated with their hardness [7], which is in good agreement with the above results. In addition, when $x = 0.5$, the $CoCrFeNi_2Mo_{0.5}$ high-entropy alloy coating has the smallest friction coefficient (0.63), widths/depths of worn tracks (width: 803.690 μm; depth: 20.630 μm), and wear rate (5.136×10^{-5} $mm^3/(N\cdot m)$). And its wear rate is one order of magnitude smaller than that of TC4 substrate material (3.694×10^{-4} $mm^3/(N\cdot m)$), demonstrating the best wear resistance. This is mainly because the appropriate proportion of hard α-Ti and σ phases in the $CoCrFeNi_2Mo_{0.5}$ high-entropy alloy coating effectively plays a supporting role in resisting wear, while the relatively soft and dispersed BCC solid solution phase and $(Ni, Co)Ti_2$ phase can effectively prevent the occurrence of brittle fracture during wear. The combined effect of the above two makes the $CoCrFeNi_2Mo_{0.5}$ high-entropy alloy coating exhibit optimal wear resistance. In addition, it is worth mentioning that the wear resistance of the $CoCrFeNi_2Mo_{0.5}$ high-entropy alloy coating is much better than the traditional WC-14Co-3Cr [36] and $NiCr/Cr_3C_2$-10%hBN coatings [37] that have been reported; that is, the wear rate of the $CoCrFeNi_2Mo_{0.5}$ high-entropy alloy coating is nearly an order of magnitude lower than the latter two. It is a promising dry sliding wear-resistant material.

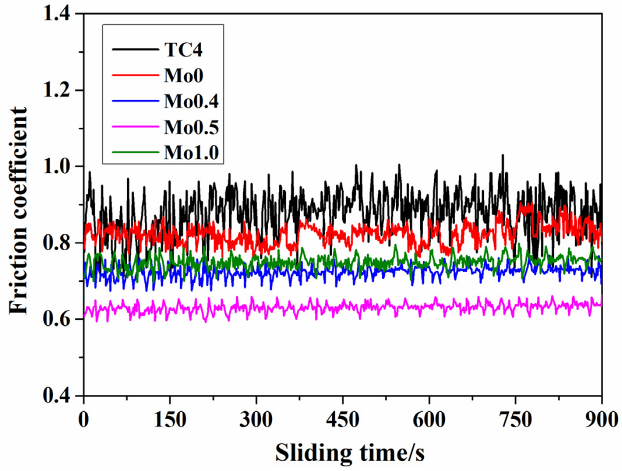

Figure 6. The friction coefficients of TC4 substrate and $CoCrFeNi_2Mo_x$ coatings.

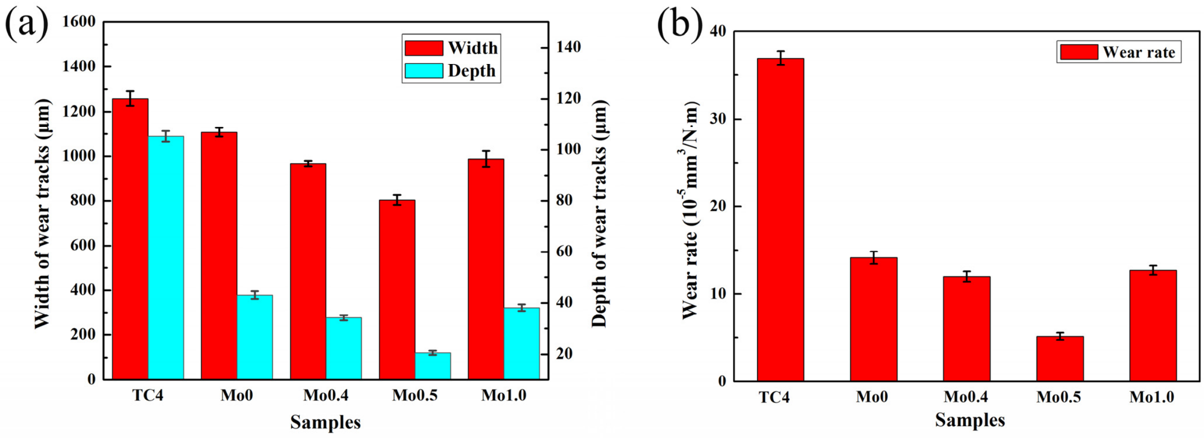

Figure 7. Wear behaviors of TC4 substrate and $CoCrFeNi_2Mo_x$ coatings: (**a**) width and depth of worn tracks, (**b**) wear rate.

Figure 9 shows the morphologies of the worn surfaces of $CoCrFeNi_2Mo_x$ high-entropy alloy coatings, and their corresponding EDS results are shown in Table 4. As shown in Figure 9a,b, when x = 0, the Mo0 coating suffers severe wear damage, and a large number of deep grooves (parallel to the friction direction) appear on the worn surface, exhibiting severe abrasive wear mechanisms. The Mo0 coating has a relatively low hardness; thus, during the friction and wear process, the hard coupled ball (Si_3N_4 ball, 1500 HV) would be embedded into the surface of the Mo0 coating for periodic and repeated cutting under the cyclic action of reciprocating sliding compressive stress, ultimately forming a large number of deep grooves parallel to the friction direction [38]. In addition, the wear characteristics of severe plastic deformation and wear pits also exist on the worn surface of Mo0 coating. In the initial stage of reciprocating sliding, there are varying degrees of local contact between the coating and the Si_3N_4 coupled ball, causing the generation of local stress and further leading to plastic deformation. At the same time, the atoms on the two contact surfaces would adhere due to the bonding of atoms during this process. As the sliding continues, the adhesive points are sheared and transferred, and further detachment occurs to form the third body abrasives. These abrasive particles come into contact with the worn surface, and under the cyclic action of reciprocating sliding compressive stress, the abrasive particles begin to roll, slide, or break on the surfaces. During this process, the contact points between the abrasive particles and the worn surfaces would change, leading to a continuous change in the trajectory of the abrasive particles. Subsequently, the force of friction is generated between the abrasive particles and the worn surfaces, which causes the abrasive particles to create indentations on the worn surfaces. As these abrasive particles continue to roll and slide, the indentation would gradually expand or connect with each other, eventually forming the wear pits. The EDS results of the worn surface shown in Table 4 illustrate that region B of the Mo0 coating contains a high content of oxygen element (56.11 at.%), indicating the presence of oxidative wear. This is because a large amount of frictional heat is generated between the coating and the coupled ball during the friction and wear process. The relatively soft Mo0 coating is subjected to repeated cutting of the coupled Si_3N_4 ball, leading to the generation of debris, which is easily in contact with the oxygen in the air and undergoes oxidation, forming an oxide film under repeated sliding actions. However, once the oxide films are formed, it would be rapidly destroyed, and so the cycle is repeated, accompanied by the entire friction and wear process. With the increase in x, no plastic deformation and wear pits appeared on the surface of Mo0.4 and Mo0.5 coatings, only some plow grooves parallel to the direction of frictional wear are presented, demonstrating the wear mechanism of abrasive wear. In addition, as x further increases to 1.0, the surface of Mo1.0 coating shows more severe wear and damage characteristics. Similar to the Mo0 coating, the Mo1.0 surface has deep plow grooves, plastic deformation, and wear pits, exhibiting the wear mechanisms of abrasive wear and plastic deformation. And as shown in Table 4, the oxygen content of region D in Mo1.0 (52.81 at.%) is very high, indicating the existence of an oxidative wear mechanism.

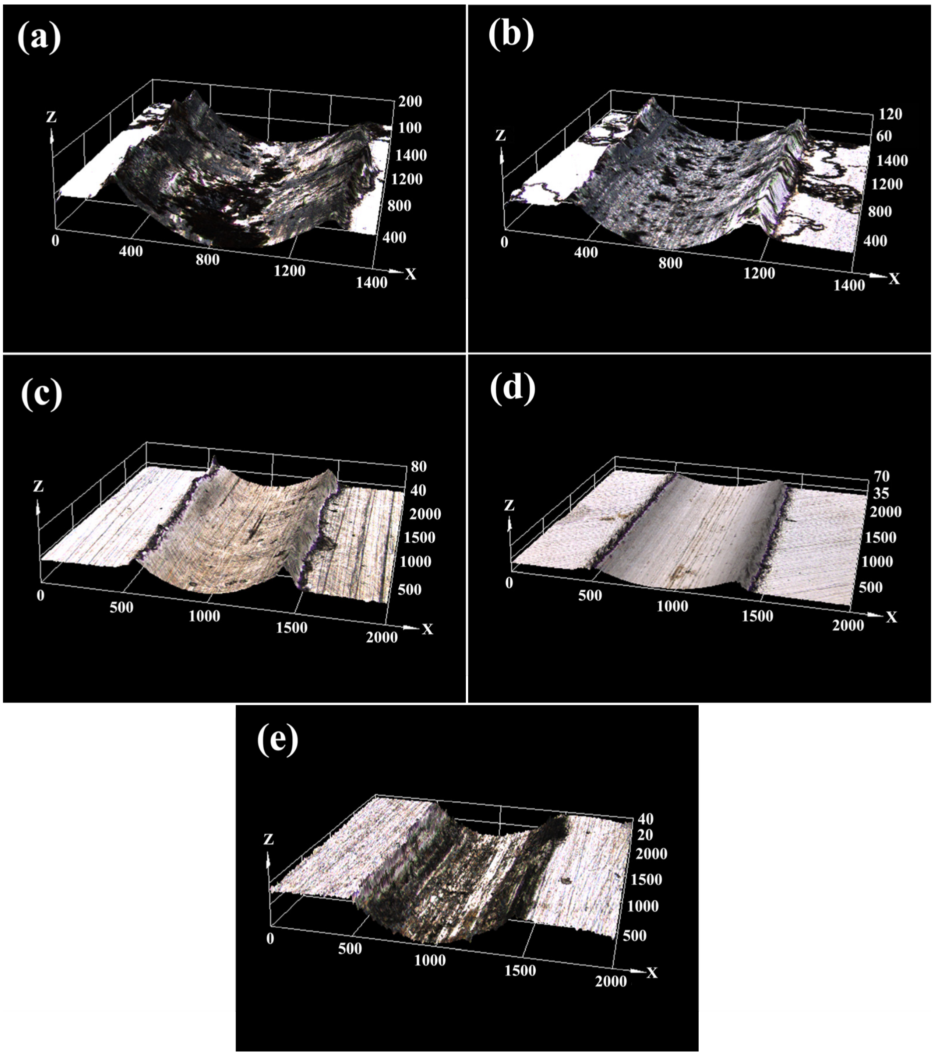

Figure 8. Three-dimensional worn morphologies of samples: (**a**) TC4 substrate, (**b**) Mo0, (**c**) Mo0.4, (**d**) Mo0.5, (**e**) Mo1.0.

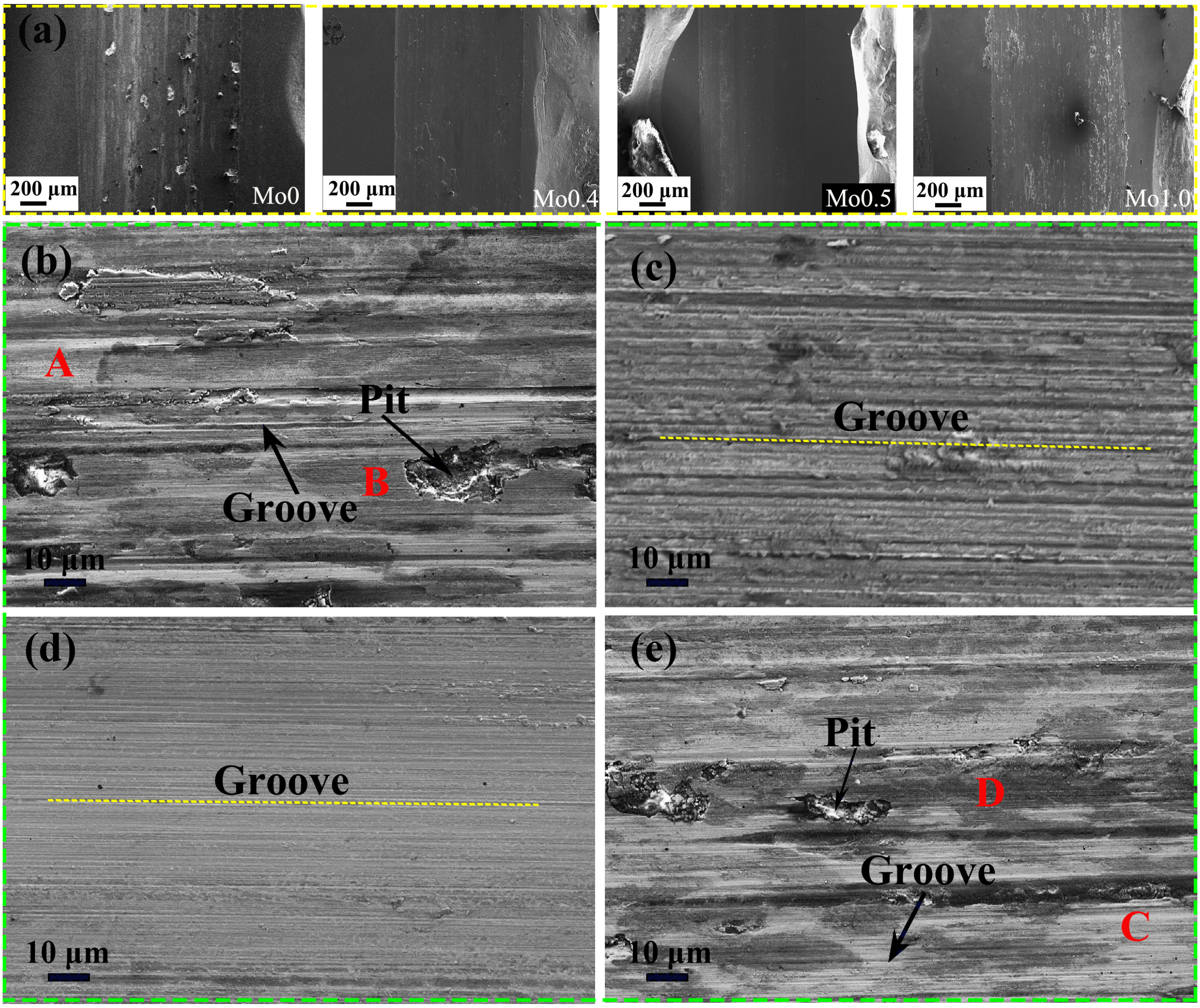

Figure 9. Worn surfaces of CoCrFeNi$_2$Mo$_x$ coatings: (**a**) SEM images of the entire worn tracks, (**b**–**e**) the worn surfaces of Mo0, Mo0.4, Mo0.5, and Mo1.0, respectively.

Table 4. The chemical compositions of worn surfaces of CoCrFeNi$_2$Mo$_x$ coatings (at.%).

Sample	Region	Co	Cr	Fe	Ni	Mo	Ti	O
Mo0	A	18.20	19.13	18.84	35.46	…	3.86	4.51
	B	8.37	7.93	8.16	14.84	…	4.59	56.11
Mo0.4	Entirety	17.86	16.72	18.10	34.14	7.28	3.51	2.39
Mo0.5	Entirety	16.95	17.66	17.83	32.66	8.70	3.12	3.08
Mo1.0	C	16.13	16.44	15.81	30.03	16.20	3.26	2.13
	D	7.81	6.97	7.73	15.50	7.62	1.56	52.81

4. Conclusions

In this article, the CoCrFeNi$_2$Mo$_x$ (x = 0, 0.4, 0.5, 1.0, x values in atomic ratio) high-entropy alloy coatings were designed and prepared using laser cladding technology, the microstructures and dry sliding wear resistance of coatings were studied in detail, and some important conclusions obtained were as follows:

(1) The $CoCrFeNi_2Mo_x$ high-entropy alloy coatings were divided vertically from top to bottom into cladding zone, bonding zone, heat affected zone, and substrate. The coatings all showed the typical dendritic morphology. When $x < 0.4$, the coatings were mainly composed of BCC solid solution phase, (Ni, Co)Ti_2 phase, and α-Ti phase. When $x \geq 0.4$, the new σ phase appeared in the coatings.

(2) The average hardness values of Mo0, Mo0.4, Mo0.5, and Mo1.0 coatings were 785 HV, 850 HV, 882 HV, and 813 HV, respectively, which was much higher than the hardness of the TC4 substrate (about 320 HV), almost 2.45–2.65 times that of the substrate. In addition, as the Mo content increased from 0 to 1.0, the hardness showed a trend of first increasing and then decreasing. Especially when $x = 0.5$, the $CoCrFeNi_2Mo_{0.5}$ high-entropy alloy coating hardness reached a maximum (882 HV), which was 2.65 times the hardness of the TC4 substrate.

(3) The friction and wear behaviors of all $CoCrFeNi_2Mo_x$ high-entropy alloy coatings were much more excellent than those of the TC4 substrate material, indicating that the coatings had a significant effect on improving the wear resistance of the TC4 substrate. As for the $CoCrFeNi_2Mo_x$ high-entropy alloy coatings, with the increase in Mo content, the widths/depths of worn tracks, wear rates, and friction coefficients of the $CoCrFeNi_2Mo_x$ high-entropy alloy coatings showed a trend of first decreasing and then increasing.

(4) When $x = 0.5$, the $CoCrFeNi_2Mo_{0.5}$ high-entropy alloy coating had the smallest friction coefficient (0.63), widths/depths of worn tracks (width: 803.690 μm; depth: 20.630 μm), and wear rate (5.136×10^{-5} $mm^3/(N \cdot m)$), which was one order of magnitude smaller than that of substrate (3.694×10^{-4} $mm^3/(N \cdot m)$), demonstrating the best wear resistance, which was mainly due to the appropriate proportion of hard α-Ti and σ phases effectively played a supporting role in resisting wear, while the relatively soft and dispersed BCC and (Ni, Co)Ti_2 phases could effectively prevent the occurrence of brittle fracture during wear.

Author Contributions: Methodology, Y.L., H.L. and J.H.; data curation, software, J.L., L.J. and H.X.; investigation, H.L. and Y.L.; formal analysis, H.L. and H.X.; conceptualization, Z.C., J.L. and L.J.; writing—original draft, H.L., J.H. and Y.L.; writing—review and editing, H.L., Z.C. and Y.L.; funding acquisition, Z.C., L.J. and H.L. All authors have read and agreed to the published version of the manuscript.

Funding: The authors thank the National Natural Science Foundation of China (Nos. 52301049, 52271024, and 52101036), the Technology Talent Innovation Support Policy Project Plan of Dalian (No. 2022RQ053), and the National Key Research and Development Program of China (No. 2018YFE0306103).

Institutional Review Board Statement: Not applicable.

Informed Consent Statement: Not applicable.

Data Availability Statement: Data are contained within the article.

Conflicts of Interest: The authors declare no conflict of interest.

References

1. Qiu, M.; Qian, Y. *Principle and Design of Tribology*; National Defense Industry Press: Beijing, China, 2013.
2. Kusinski, J.; Kac, S.; Kopia, A.; Radziszewska, A.; Rozmus-Górnikowska, M.; Major, B.; Major, L.; Marczak, J.; Lisiecki, A. Laser modification of the materials surface layer—A review paper. *Bull. Pol. Acad. Sci. Tech. Sci.* **2012**, *60*, 711–728. [CrossRef]
3. Huang, C.; Zhang, Y.; Vilar, R.; Shen, J. Dry sliding wear behavior of laser clad TiVCrAlSi high entropy alloy coatings on Ti-6Al-4V substrate. *Mater. Des.* **2012**, *41*, 338–343. [CrossRef]
4. Han, B.; Zhang, M.; Qi, C.; Cui, N.; Wang, Y. Characterization and friction-reduction performances of composite coating produced by laser cladding and ion sulfurizing. *Mater. Lett.* **2015**, *150*, 35–38. [CrossRef]
5. Yang, M.; Liu, X.-B.; Fan, J.-W.; He, X.-M.; Shi, S.-H.; Fu, G.-Y.; Wang, M.-D.; Chen, S.-F. Microstructure and wear behaviors of laser clad NiCr/Cr_3C_2-WS_2 high temperature self-lubricating wear-resistant composite coatings. *Appl. Surf. Sci.* **2012**, *258*, 3757–3762. [CrossRef]

6. Kafali, M.; Doleker, K.M.; Erdogan, A.; Sunbul, S.E.; Icin, K.; Yildiz, A.; Gok, M.S. Wear, corrosion and oxidation characteristics of consolidated and laser remelted high entropy alloys manufactured via powder metallurgy. *Surf. Coat. Technol.* **2023**, *467*, 129704. [CrossRef]
7. Shang, C.; Axinte, E.; Sun, J.; Li, X.; Li, P.; Du, J.; Qiao, P.; Wang, Y. CoCrFeNi($W_{1-x}Mo_x$) high-entropy alloy coatings with excellent coatings with excellent mechanical properties and corrosion resistance prepared by mechanical alloying and hot pressing sintering. *Mater. Des.* **2017**, *117*, 193–202. [CrossRef]
8. Guo, S.; Wang, M.; Wang, Q.; Sui, S.; Kayani, S.H.; Seol, J.B.; Zhu, P.; Guo, A.; Lin, X.; Huang, W. The influence of chemical short-range order on the nanoindentation properties of high-entropy alloys prepared via laser powder bed fusion. *Mater. Charact.* **2024**, *207*, 113560. [CrossRef]
9. Komarasamy, M.; Kumar, N.; Tang, Z.; Mishra, R.S.; Liaw, P.K. Effect of microstructure on the deformation mechanism of frictin stri-processed $Al_{0.1}$CoCrFeNi high entropy alloy. *Mater. Res. Lett.* **2015**, *3*, 30–34. [CrossRef]
10. Yang, X.; Zhang, Y. Preparation of high-entropy stabilized solid solution in multi-component alloys. *Mater. Phys. Chem.* **2012**, *132*, 233–238. [CrossRef]
11. Wu, P.H.; Liu, N.; Yang, W.; Zhu, Z.X.; Lu, Y.P.; Wang, X.J. Microstructure and solidification behavior of multicomponent $CoCrCu_xFeMoNi$ high-entropy alloys. *Mater. Sci. Eng. A* **2015**, *642*, 142–169. [CrossRef]
12. Tang, W.; Yeh, J. Effect of aluminum content on plasma-nitrided $Al_xCoCrCuFeNi$ high-entropy alloys. *Metall. Mater. Trans. A* **2009**, *40*, 1479–1486. [CrossRef]
13. Erdogan, A.; Sunbul, S.E.; Icin, K.; Doleker, K.M. Microstructure, wear and oxidation behavior of AlCrFeNiX (X = Cu, Si, Co) high entropy alloys produced by powder metallurgy. *Vac. Technol. Appl. Ion Phys.* **2021**, *187*, 110143. [CrossRef]
14. Wang, Y.; Yang, Y.; Yang, H.; Zhang, M.; Qiao, J. Effect of nitriding on the tribological properties of $Al_{1.3}CoCuFeNi_2$ high entropy alloy. *J. Alloys Compd.* **2017**, *725*, 365–372. [CrossRef]
15. Licavoli, J.J.; Gao, M.C.; Sears, J.S.; Jablonski, P.D.; Hawk, J.A. Microstructure and mechanical behavior of high entropy alloys. *J. Mater. Eng. Perform.* **2017**, *114*, 253–263. [CrossRef]
16. Chen, Y.; Zhu, S.; Wang, X.; Han, G.; Qiu, L. Laser cladding $Al_{0.4}CoCu_{0.6}NiSi_{0.2}Ti_{0.25}$ layer of abrasion resistance and high entropy alloys forming mechanism analysis. *Hot Work. Technol.* **2018**, *47*, 1–6.
17. Qi, P.; Liang, X.; Tong, Y.; Chen, Y.; Zhang, Z. Preparation and characterization of NbMoTaW high entropy alloy coating. *Appl. Laser* **2018**, *38*, 382–386.
18. Zheng, B.; Wei, J.; Jiang, Y.; Zhang, X. Study on wear resistance of NiCoFeCrTi high entropy alloy coating by laser cladding. *Laser Technol.* **2016**, *40*, 432–435.
19. Huang, Y.; Hu, Y.; Zhang, M.; Mao, C.; Tong, Y.; Zhang, J.; Li, K.; Wang, K. On the enhanced wear resistance of laser-clad $CoCrCuFeNiTi_x$ high-entropy alloy coatings at elevated temperature. *Tribol. Int.* **2022**, *174*, 107767. [CrossRef]
20. Wu, W.; Jiang, L.; Jiang, H.; Pan, X.; Cao, Z.; Deng, D.; Wang, T.; Li, T. Phase evolution and properties of $Al_2CrFeNiMo_x$ high-entropy alloys coatings by laser cladding. *J. Therm. Spray Technol.* **2015**, *24*, 1333–1340. [CrossRef]
21. Luo, J.; Sun, W.; Duan, R.; Yang, W.; Chan, K.C.; Ren, F.; Yang, X.-S. Laser surface treatment-introduced gradient nanostructured TiZrHfTaNb refractory highentropy alloy with significantly enhanced wear resistance. *J. Mater. Sci. Technol.* **2022**, *110*, 43–56. [CrossRef]
22. Li, H.-G.; Che, P.-C.; Yang, X.-K.; Huang, Y.-J.; Ning, Z.-L.; Sun, J.-F.; Fan, H.-B. Enhanced tensile properties and wear resistance of additively manufactured CoCrFeMnNi high-entropy alloy at cryogenic temperature. *Rare Met.* **2022**, *41*, 1210–1216. [CrossRef]
23. Jiang, L.; Lu, Y.; Wu, W.; Cao, Z.; Li, T. Microstructure and mechanical properties of a $CoFeNi_2V_{0.5}Nb_{0.75}$ eutectic high entropy alloy in as-cast and heat-treated conditions. *J. Mater. Sci. Technol.* **2016**, *32*, 245–250. [CrossRef]
24. Xiong, F.; Wu, Y.; Liu, X.; Wang, H.; Jiang, S.; Zhang, X.; Lu, Z. Enhancing cryogenic yield strength and ductility of the $Al_{0.1}$CoCrFeNi high-entropy alloy by synergistic effect of nanotwins and dislocations. *Scr. Mater.* **2023**, *232*, 115495. [CrossRef]
25. Zhou, Y.J.; Zhang, Y.; Wang, Y.L.; Chen, G.L. Solid solution alloys of $AlCoCrFeNiTi_x$ with excellent room-temperature mechanical properties. *Appl. Phys. Lett.* **2007**, *90*, 181904. [CrossRef]
26. Qiu, X.W.; Liu, C.G. Microstructure and properties of $Al_2CrFeCoCuTiNi_x$ high-entropy alloys prepared by laser cladding. *J. Alloys Compd.* **2013**, *553*, 216–220. [CrossRef]
27. Cai, Y.C.; Chen, Y.; Luo, Z.; Gao, F.; Li, L. Manufacturing of $FeCoCrNiCu_x$ medium-entropy alloy coating using laser cladding technology. *Mater. Des.* **2017**, *133*, 91–108. [CrossRef]
28. Zhang, H.; Pan, P.; He, Y.Z. Synthesis and characterization of FeCoNiCrCu high-entropy alloy coating by laser cladding. *Mater. Des.* **2011**, *32*, 1910–1915. [CrossRef]
29. Song, R.; Ye, F.; Yang, C.; Wu, S. Effect of alloying elements on microstructure, mechanical and damping properties of Cr-Mn-Fe-V-Cu high-entropy alloys. *J. Mater. Ence Technol.* **2018**, *34*, 2014–2021. [CrossRef]
30. Han, L.I. Microstructure and properties of laser cladding $AlB_xCoCrNiTi$ high-entropy alloy coating on titanium alloys. *Surf. Technol.* **2017**, *46*, 226–231.
31. Chou, Y.L.; Yeh, J.W.; Shih, H.C. The effect of molybdenum on the corrosion behaviour of the high-entropy alloys $Co_{1.5}CrFeNi_{1.5}Ti_{0.5}Mo_x$ in aqueous environments. *Corros. Sci.* **2010**, *52*, 2571–2581. [CrossRef]
32. Tao, T.S.; Liang, Y.C.; Ming, H.C. Microstructure and mechanical properties of multiprincipal component $CoCrFeNiMo_x$ alloys. *Mater. Charact.* **2012**, *60*, 63–67.

33. Liu, W.H.; Lu, Z.P.; He, J.Y.; Luan, J.; Wang, Z.; Liu, B.; Liu, Y.; Chen, M.; Liu, C. Ductile CoCrFeNiMo$_x$ high entropy alloys strengthened by hard intermetallic phases. *Acta Mater.* **2016**, *116*, 332–342. [CrossRef]
34. Dong, Y.; Jiang, L.; Jiang, H.; Lu, Y.; Wang, T.; Li, T. Effects of annealing treatment on microstructure and hardness of bulk AlCrFeNiMo$_{0.2}$ eutectic high-entropy alloy. *Mater. Des.* **2015**, *82*, 91–97. [CrossRef]
35. Zhang, S.; Wu, C.L.; Zhang, C.H.; Guan, M.; Tan, J. Laser surface alloying of FeCoCrAlNi high-entropy alloy on 304 stainless steel to enhance corrosion and cavitation erosion resistance. *Opt. Laser Technol.* **2016**, *84*, 23–31. [CrossRef]
36. Staia, M.H.; Carrasquero, E. Wear behaviour of HVOF thermally sprayed WC-14Co-3Cr coatings. *Surf. Eng.* **2013**, *16*, 515–518. [CrossRef]
37. Cao, Y.; Huang, C.; Du, L.; Zhang, W.; Lan, Y. Preparation and tribological properties of atmospheric plasma-sprayed NiCr/Cr$_3$C$_2$-hBN wear-resistant coatings. *Surf. Technol.* **2015**, *44*, 27–31.
38. Liang, J.; Yin, X.Y.; Lin, Z.Y.; Chen, S.; Liu, C.; Wang, C. Microstructure and wear behaviors of laser cladding in-situ synthetic (TiB$_x$+TiC)/(Ti$_2$Ni+TiNi) gradient composite coatings. *Vacuum* **2020**, *176*, 109305. [CrossRef]